Performance and operating limits of a sorbent-catalyst system for sorption-enhanced reforming (SER) in a fluidized bed reactor

Isabel Martínez[1], Gemma Grasa[1], Julien Meyer[2], Luca Di Felice[2], Saima Kazi[2], Cristina Sanz[2], Delphine Maury[3], Christophe Voisin[3]*

[1]Instituto de Carboquímica, Spanish Research Council (ICB-CSIC), Miguel Luesma Castán 4, 50018, Zaragoza, Spain

[2]Institute for Energy Technology (IFE), P.O. Box 40, 2027 Kjeller, Norway

[3]Marion Technologies, 55 rue Louis Pasteur, 09340 Verniolle, France
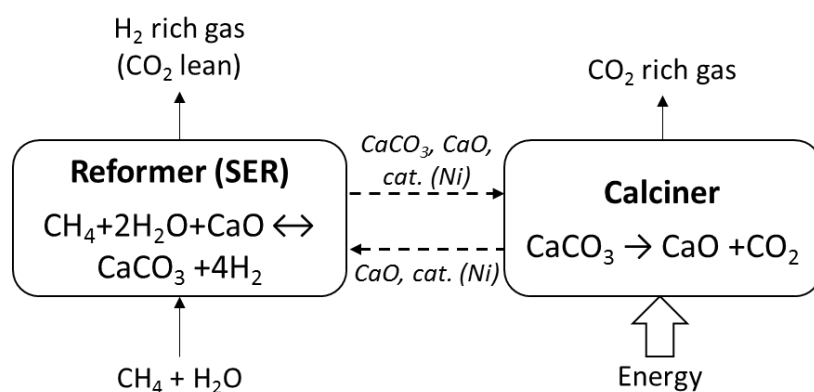
*corresponding author, imartinez@icb.csic.es

Abstract

The combined performance of a synthetic $CaO-Ca_{12}Al_{14}O_{33}$ sorbent and an $Ni-MgAl_2O_4$ reforming catalyst was tested in a fluidized bed reactor under relevant operating conditions for the sorption-enhanced reforming (SER) process. The effect of CH_4 space velocity (i.e. $kg_{CH4}/h \cdot kg_{cat}$), steam-to-carbon (S/C) ratio and superficial gas velocity on product gas composition was assessed, as well as the effect of regeneration conditions on material performance. Moreover, a bi-functional material prepared by mechanical mixing of the separate materials was also tested in the reactor under consecutive SER/regeneration cycles. H_2 contents as high as 96 vol% (N_2 free, dry basis) were achieved under SER operation, using the separated materials working with an Ni content of 3.75 wt% in the solid bed at 650 ºC with S/C ratios of 3 and 4. This solid system is able to process up to 0.63 $kg_{CH4}/h \cdot kg_{cat}$ at 0.1 m/s superficial gas velocity and with an S/C ratio of 4, although the CH_4 input has to be reduced to 0.33 $kg_{CH4}/h \cdot kg_{cat}$ when working with a lower S/C ratio. Similar H_2 contents to those found in the separated materials were obtained with the combined sorbent-catalyst material working with 0.33 $kg_{CH4}/h \cdot kg_{cat}$ at 0.1 m/s superficial gas velocity and S/C ratios of 3 and 4. The CO_2 sorption capacity of the combined material produced the same as that of the separate sorbent particles (i.e. around 0.25 g_{CO2}/g calcined sorbent), while remaining stable throughout the SER/regeneration cycles.

Keywords: sorption enhanced reforming, hydrogen production, CO_2 sorbent, functional combined materials, fluidized bed reactor

1. Introduction

Large-scale hydrogen production from natural gas, including CO_2 capture, transport and storage, is seen as a viable mechanism to contribute to the decarbonization of the power, heat and oil & gas sectors, in addition to a number of other industries, including ammonia and steel production (Edenhofer et al., 2014). Moreover, decarbonized hydrogen can also be introduced as a zero-emissions fuel for transport in the near future. In this context, large-scale hydrogen production processes, including CO_2 capture at a reduced cost and more efficiently than through existing processes, provides a great opportunity to contribute to climate change mitigation (IEA, 2006).

One of the most promising new technologies for the production of hydrogen with integrated CO_2 capture is the sorption-enhanced reforming (SER) of natural gas (Han and Harrison, 1994; Harrison, 2008). The SER process relies on a high-temperature solid looping cycle that involves a CaO-based CO_2 sorbent and a reforming catalyst. The configuration of the system generally requires the use of two reactors with a circulation of solids between them, as depicted in Figure 1. Methane reforming (Eq. 1), water-gas shift (Eq. 2) and CO_2 capture (via carbonation of CaO) (Eq. 3) reactions occur simultaneously in the reformer reactor when feeding CH_4 (usually as natural gas) and steam in the presence of a solid stream containing CaO and a reforming catalyst. Solids exiting the reformer contain $CaCO_3$ and unconverted CaO, and are sent to a second reactor (calciner or regenerator) where the carbonated sorbent is heated up to release a near-to-pure CO_2 gas stream ready for compression and further storage and/or utilization. Compared to conventional steam methane reforming (SMR), SER significantly reduces the four process steps (reforming, high-temperature and low-temperature water-gas shift reactions and CO_2 separation) to one integrated system with only two reaction vessels, allowing interconnected fluidized bed reactors to be used. Moreover, a full-scale H_2 production plant based on the SER process has demonstrated hydrogen production efficiencies of between 9 and 15 percentage points higher than an SMR-based plant with CO_2 capture using amines (Martínez et al., 2013). Therefore, the SER process has the potential to reduce the cost of hydrogen production by process intensification and energy savings, and may, in the medium term, contribute to a more efficient and profitable production of hydrogen with integrated CO_2 capture.

$$CH_4 + H_2O \leftrightarrow CO + 3H_2 \qquad \Delta H_{298\,K} = +206.2\ kJ/mol \qquad (1)$$

$$CO + H_2O \leftrightarrow CO_2 + H_2 \qquad \Delta H_{298\,K} = -41.5\ kJ/mol \qquad (2)$$

$$CaO + CO_2 \leftrightarrow CaCO_3 \qquad \Delta H_{298\,K} = -178.8\ kJ/mol \qquad (3)$$

Figure 1 Schematic of the sorption-enhanced reforming process

The SER process has been proposed for series of fixed bed reactors operating in parallel (Abanades et al., 2010; Li et al., 2006b; Waldron et al., 2001), or in a dual fluidized bed system by circulating the solids between two reactors operating in steady state (Arstad et al., 2012, 2009; Johnsen et al., 2006). For continuous process operation, the sorbent requires regeneration. Several alternatives appear in the literature to provide the energy required by the highly endothermic calcination (or regeneration) step, such as by directly burning a fuel in an O_2-rich atmosphere (Ochoa-Fernandez et al., 2007; Romano et al., 2011), by coupling the exothermic reduction reaction of a metal oxide in the regenerator (Antzara et al., 2015; Fernández et al., 2012; Zhu and Fan, 2015), and by indirectly using an integrated high-temperature heat exchanger in the regenerator (Meyer et al., 2011).

The CO_2 sorbent represents the core of the process. CaO-based CO_2 sorbents have been identified as suitable materials for the SER process due to their relatively low cost, high availability, fast kinetics and high capacity for CO_2 capture (Di Giuliano and Gallucci, 2018). Most of the experimental investigation into the SER process has focused on natural sorbents, such as limestone and dolomite (Arstad et al., 2012; Hildenbrand et al., 2006; Johnsen et al., 2006; Lopez Ortiz and Harrison, 2001; Yi and Harrison, 2005). However, CaO-based materials derived from natural precursors suffer from a rapid decrease in CO_2 uptake capacity over repeated carbonation/calcination cycles due to the effects of sintering and pore closure, and they present poor mechanical properties. For the purpose of overcoming the diminishing CO_2 capture capacity presented by CaO-based sorbents derived from natural limestones and dolomites, there has been an intense research in the recent years into the development of synthetic CaO-based sorbents. The aim is to produce materials that are highly resistant to sintering and with the sufficient CO_2 sorption capacity and reactivity to sustain Ca-looping processes (see reviews from Erans et al. (2016), Shokrollahi Yancheshmeh et al. (2016) and Yin et al. (2012) for more information). Advanced synthetic materials with improved chemical and mechanical stability compared to natural sorbents have the potential to reduce the capital and operating costs required by SER, and therefore represent an important economic stimulus for advancing SER technology towards up-

scaling and commercialization. CaO dispersed onto porous supports that are stable at high temperature, such as calcium aluminates, has been extensively studied over the last decade. Complex and expensive preparation methods such as sol-gel or flame spray pyrolysis have little potential for upscaling, whereas hydrothermal synthesis, co-precipitation and wet mixing may offer cost-effective pathways. A $CaO/Ca_{12}Al_{14}O_{33}$ sorbent produced from low-cost hydroxide precursors by a hydrothermal method has shown outstanding stability (21 g_{CO2}/100 g sorbent) for up to 40 cycles (Kazi et al., 2014). To produce this sorbent, CaO was finely dispersed onto a micro-porous mayenite structure, preventing sintering and achieving a highly stable sorption capacity. Recent work has also been devoted to the integration of a reforming catalyst within a sorbent structure in a so-called bi-functional combined sorbent-catalyst material (CSCM). The aim of this CSCM is improving mass transfer and reaction kinetics, while avoiding particle segregation, facilitating material reprocessing and lowering the material production cost, and therefore improving the overall techno-economic performance of the SER process (Cesário et al., 2015; Chanburanasiri et al., 2011; Di Giuliano et al., 2017; Kalantzopoulos et al., 2015; Martavaltzi and Lemonidou, 2010).

The proof of concept of the SER process in a fluidized bed reactor has been successfully validated using natural calcined dolomite as sorbent (Arstad et al., 2012; Johnsen et al., 2006), but there is very little experimental work available that covers the SER performance of new synthetic CaO-based sorbents in fluidized bed reactors. Typically, the performance of synthetic CaO-based sorbents in SER processes has been explored in fixed bed reactors aiming at determining the operation limits of both individual sorbent particles and bi-functional (sorbent-catalyst) materials (Aloisi et al., 2017; García-Lario et al., 2015a, 2015b; Martavaltzi et al., 2011). In this context, the aim of this work was to determine the performance and operation limits of a $CaO-Ca_{12}Al_{14}O_{33}$ sorbent and reforming catalyst mixture in a fluidized bed reactor under relevant SER operating conditions. These operating limits were assessed with regard to the maximum CH_4 space velocity that the 2-particle system used in this work (e.g. sorbent-to-catalyst mass ratio of 3) was able to process for a given amount of steam fed to the reactor. The experimental work was conducted considering an SER configuration making use of indirect heat transfer inside the regenerator, and therefore the sorbent was regenerated in a highly oxidizing, steam-rich atmosphere. In order to prevent any catalyst deactivation due to oxidation while sorbent regeneration was taking place, a minimum presence of H_2 was required in the regenerator. The amount of H_2 required to preserve the catalyst from oxidation was experimentally determined. Finally, the performance of this 2-particle system was compared to that of a CSCM based on the same sorbent and catalyst materials.

2. Experimental section

2.1. Materials description

Two functional materials were required to test SER, the CO_2 sorbent and the reforming catalyst. In this case, the sorbent used was a CaO-based material supported on mayenite ($Ca_{12}Al_{14}O_{33}$). This inert frame was revealed to be a suitably stable support for CaO-based sorbent materials operating in the temperature range of interest for the process (i.e. 600–925 ºC) (Kazi et al., 2014; Li et al., 2006a; Mastin et al., 2011; Zamboni et al., 2015). The CaO-$Ca_{12}Al_{14}O_{33}$ sorbent powder contained 30 wt% CaO and 70 wt% $Ca_{12}Al_{14}O_{33}$, and it was prepared according to the hydrothermal synthesis route reported by Kazi et al. (2014) using calcium hydroxide ($Ca(OH)_2$, Balthazard & Cotte) and aluminium hydroxide ($Al(OH)_3$, Alumines Durmax SG27) as precursors. Stoichiometric amounts of the precursors were weighed in a stainless steel autoclave reactor and mixed together with demineralized water at a liquid/solid weight ratio equal to 3. The slurry was heated to 150 ºC for 4 hours at a pressure of between 3 and 4 bar. The product from the autoclave was then cooled, centrifuged and dried in a heating cabinet at 100 ºC. At this stage, the product contained $Ca(OH)_2$ and calcium aluminium hydroxide $Ca_3Al_2(OH)_{12}$. The dried powder was then granulated in several consecutive steps using a high shear granulator (GUEDU 90NO/PO) and a solution of 10 wt% polyvinyl alcohol as binder. The wet sorbent granules were dried at 100 ºC and then calcined in air at 1000 ºC for 1 hour in a high-temperature furnace. Finally, after cooling, the CaO-$Ca_{12}Al_{14}O_{33}$ material was sieved to obtain granules between 200 and 300 µm. The reforming catalyst used in this study was a commercial catalyst provided by Haldor Topsøe AS, Denmark, and contained 15 wt% Ni on a magnesium aluminate spinel ($MgAl_2O_4$) as support. The catalyst was crushed and sieved to obtain both a powder with particle size below 122 µm and particles with an average size of 150 µm.

These materials were tested in the fluidized bed reactor described below, separately, which we refer to as the '*2-particle system*', and combined as a CSCM material, which we refer to as the '*1-particle system*'. The CSCM material was produced by the mechanical mixing of the CaO-$Ca_{12}Al_{14}O_{33}$ material and reforming catalyst powders. The CaO-$Ca_{12}Al_{14}O_{33}$ powder, after heat treatment at 1000 ºC in air during 1 hour, was mechanically mixed with the catalyst powder using a sorbent-to-catalyst weight ratio equal to 1.5. The mixed powders were then granulated in several consecutive steps using a high shear granulator (GUEDU 90NO/PO) and a solution of 10 wt% polyvinyl alcohol as binder. The wet CSCM granules were dried at 100 ºC and then calcined in air at 800 ºC for 3 hours in a high-temperature furnace to remove the organic binder and increase the mechanical strength of the granules. Finally, after cooling, the CSCM material was sieved to obtain granules between 150 and 250 µm. The CaO-$Ca_{12}Al_{14}O_{33}$ sorbent and the CSCM material were produced by Marion Technologies at kilogram scale for characterization, thermo-gravimetric multi-cycle tests and fluidized bed reactor tests. The composition of the different materials used in this work has been summarized in Table 1.

Table 1 Composition and particle size of the functional materials tested

Material	Particle size [μm]	Composition (wt%)				
		CaO	$Ca_{12}Al_{14}O_{33}$	$MgAl_2O_4$	Ni	Al_2O_3
CaO-$Ca_{12}Al_{14}O_{33}$ sorbent (calcined form)	250	30	70	-	-	-
Commercial reforming catalyst (reduced form)	150			83.5	13.1	3.4
CSCM material (calcined and reduced form)	175	18	42	34	6	-

2.2. Materials characterisation

Physical and textural characterisation of the materials used in this work (i.e., CaO-$Ca_{12}Al_{14}O_{33}$ sorbent, commercial catalyst and CSCM) has been reported in a recent published work of the same authors, where the synthesis and performance of the referred materials were presented for the first time (Di Felice et al., 2019). In such published work, the materials were deeply characterised before and after testing (up to 100 reaction cycles) in a thermogravimetric analyser (TGA) to correlate their activity and physicochemical properties under different regeneration conditions (temperature and gas composition). The main findings from that work served to design the sequence of reaction steps incorporated in the experimental routines performed in the fluidized bed reactor, which are described in the next section. As an example, performing regeneration at 850 ℃ with a gas containing 43 vol% H_2O and 3 vol% H_2 (in N_2) allowed maintaining, for the 2-particle system, the sorbent and catalytic activity of the materials along the reaction cycles performed in the TGA. In contrast, it was necessary to avoid H_2O (by replacing it with CO_2) during the regeneration of the CSCM material to maintain its catalytic activity, and to incorporate a reduction step at high temperature (50 vol% H_2 in N_2 at 850 ℃) that helped to avoid the Ni Crystal size growth with the reaction cycles (Di Felice et al., 2019).

The textural characterization is summarized in Table 2. The intra-particle porosity of the materials was determined by Hg porosimetry and solid density by He pycnometry. N_2-adsorption was used to calculate the sorbent surface area by applying the Brunauer−Emmett−Teller (BET) equation. As shown in this table, the granulated sorbent and CSCM materials had quite a high intra-particle porosity ranging between about 62 and 67% for the calcined/reduced forms, similar to the values found in the literature for synthetic CaO-based sorbents produced through granulation (López et al., 2018). This high porosity favours the access and release of CO_2 into and from the material, resulting in good sorption kinetics in the fast reaction regime where gas diffusion through the solid does not play an important role. The surface area of the CSCM, similar to the areas reported in the literature for hybrid sorbent-catalyst materials (García-Lario et al., 2015c; Martavaltzi and Lemonidou, 2010), increases with respect to the surface area of the sorbent itself (from 6.4 to 14.6 m^2/g), which may facilitate the activity of the bi-functional material.

Table 2 Textural characterization and crystal phases detected by XRD of the fresh functional materials tested

Material	Real density [g/cm^3]	Intra-particle porosity [%]	Calculated apparent particle density g/cm^3	Specific area [m^2/g]	Crystal phases by XRD
CaO-Ca$_{12}$Al$_{14}$O$_{33}$ sorbent (calcined form)	2.704 (0.0007)	67.1	0.890	6.47 (0.007)	CaO, Ca$_{12}$Al$_{14}$O$_{33}$
Commercial reforming catalyst (reduced form)	3.828 (0.0005)	42.37	2.206	17.25 (0.033)	Ni, MgAl$_2$O$_4$, Al$_2$O$_3$
CSCM (calcined and reduced form)	3.135 (0.001)	62.02	1.191	14.62 (0.027)	CaO, Ca$_{12}$Al$_{14}$O$_{33}$,Ni, MgAl$_2$O$_4$, MgO·NiO

Standard deviation of the density measurements (in g/cm^3) is indicated between brackets

X-Ray diffraction (XRD) analysis was performed to determine the crystalline phases present in the fresh materials as well as in the materials extracted from the fluidized bed reactor at the end of the experiments, as explained in the results section. The crystal phases detected by this technique for the three previously described fresh materials have been included in Table 2. The XRD pattern of the granulated sorbent indicated the presence of the two expected phases of free CaO and Ca$_{12}$Al$_{14}$O$_{33}$. No other phases were identified, which confirms the quality of the material. The XRD pattern of the commercial catalyst revealed the main expected phases, i.e. Ni metal and MgAl$_2$O$_4$, together with a residual Al$_2$O$_3$ phase from the synthesis process. This residual phase accounted for less than 3.5 wt% of the reduced catalyst weight as determined via XRD in this work. Finally, for the CSCM, CaO, Ca$_{12}$Al$_{14}$O$_{33}$, Ni metal and MgAl$_2$O$_4$ phases were identified. The Al$_2$O$_3$ phase, present in small concentration in the catalyst, disappeared – probably to form Ca$_{12}$Al$_{14}$O$_{33}$, by reacting with free CaO in the sorbent during the thermal treatment of the granulated material.

Finally, multi-cycle carbonation/calcination tests were carried out in a thermo-gravimetric analyser (TGA, CI Electronics) in order to determine the CO$_2$ sorption capacity of the granulated CaO-Ca$_{12}$Al$_{14}$O$_{33}$ sorbent. Carbonation was carried out in the presence of steam to operate under conditions similar to those of the SER process, and therefore to detect any effect of the steam on the sorption capacity. The carbonation period lasted 10 min at 600 ℃ using a mixture of 15 vol% CO$_2$ and 47 vol% steam balanced in N$_2$, which corresponded to a steam-to-carbon ratio of 3, whereas for the calcination a temperature of 850 ℃ was used for 3 min, involving a mixture of 30 vol% CO$_2$ and 50 vol% steam balanced also in N$_2$. Figure 2 shows the evolution of the CO$_2$ sorption capacity of the granulated sorbent up to 56 calcination/carbonation cycles obtained in TGA. As shown, the CO$_2$ sorption capacity of the sorbent was sufficiently stable at a value of around 22.5 g$_{CO2}$/100 g calcined sorbent over the 56 cycles tested, which is almost 3–4 times the residual CO$_2$ sorption capacity of CaO derived from a typical natural limestone (Erans et al., 2016; Grasa and Abanades, 2006). It can be noticed that during the first 6 cycles, the CO$_2$ sorption capacity slightly decreased from around 25.5 g$_{CO2}$/100 g calcined sorbent for cycle N=2 to the residual value. This behaviour may be due to the formation of additional Ca$_{12}$Al$_{14}$O$_{33}$ in the

sorbent particles as a combination of active CaO and residual amounts of Al_2O_3, which were below the detection limits of the XRD analysis. This result confirms the chemical stability of the granulated sorbent used in this work when undergoing cycles in operating conditions similar to those present in the SER process studied.
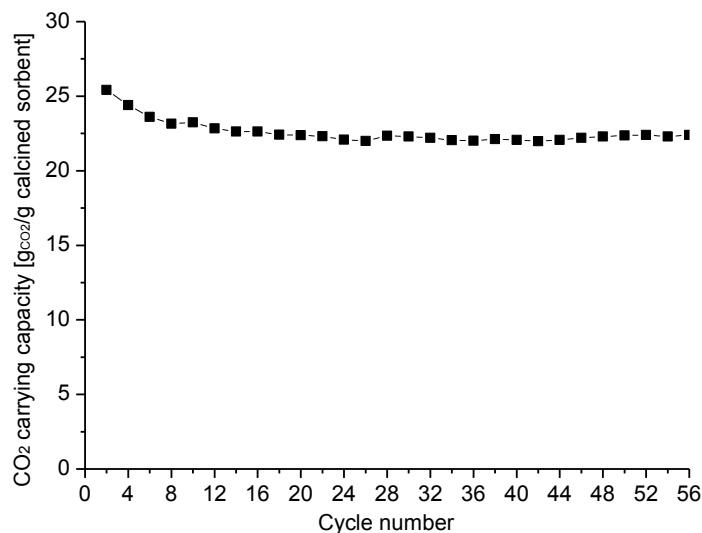
**Figure 2 CO$_2$ sorption capacity during calcination/carbonation cycles in TGA for the granulated CaO-Ca$_{12}$Al$_{14}$O$_{33}$ sorbent**

2.3. Laboratory-scale fluidized bed reactor

SER tests were carried out in the laboratory-scale fluidized bed reactor (FBR) installed at the ICB-CSIC facility, a schematic diagram of which is given in Figure 3. As previously explained in the materials description section, SER performance was evaluated using the granulated CaO-Ca$_{12}$Al$_{14}$O$_{33}$ sorbent and reforming catalyst separately, the 2-particle (2p) system, and combined, using the CSCM material in the 1-particle (1p) system. In the case of the 2p system, a sorbent-to-catalyst weight ratio equal to 3 was used, while in the case of the CSCM material, this ratio was equal to 1.5.

The fluidized bed reactor comprises an 853-mm-long tubular reactor (AISI 310), with an internal diameter of 53.1 mm, heated by an external cylindrical electric oven. The reactor has a distributor plate (located 586 mm from top reactor) with orifices covered by bubble caps. The reactor operates in batch mode for solids and it is capable of operating at temperatures above 900 ºC. The experimental system allows CH$_4$, N$_2$, CO$_2$, H$_2$ and steam to be fed into the reactor. Water is fed into the system using a pressurized vessel and a mass flow controller, and the gas mixture drowns the liquid water to pass through an evaporator unit consisting of a tubular reactor with ceramic filler, which is heated by a cylindrical electric furnace. During SER tests, a constant flow rate of N$_2$ is fed together with the CH$_4$ and H$_2$O in order to facilitate the flow of H$_2$O through the evaporator and to be used as an internal standard for quantifying the syngas flow rate at the reactor outlet. The mixture of N$_2$, CH$_4$ and steam is fed through the bottom of the fluidized bed reactor,

where reforming, water-gas shift (WGS) and carbonation reactions (Eqs. 1-3) occur. Downstream from the reactor, the product gas is cooled down in a shell-and-tube heat exchanger, using water as coolant in order to condense the H_2O present in the syngas. Finally, an aliquot of the gas stream is sent to an online gas analyser (IR-analysis and heat conductivity analysis, with an extractive analyser SICK GMS810), where the concentration of H_2, CH_4, CO and CO_2 is determined. Temperature and pressure are monitored throughout the rig as shown in Figure 3. There are three thermocouples in the fluidized bed reactor, two immersed in the bed of solids and a third one in the upper part of the reactor. The thermocouple that controls the temperature is immersed in the bed of solids and regulates the power transferred with the electric oven.
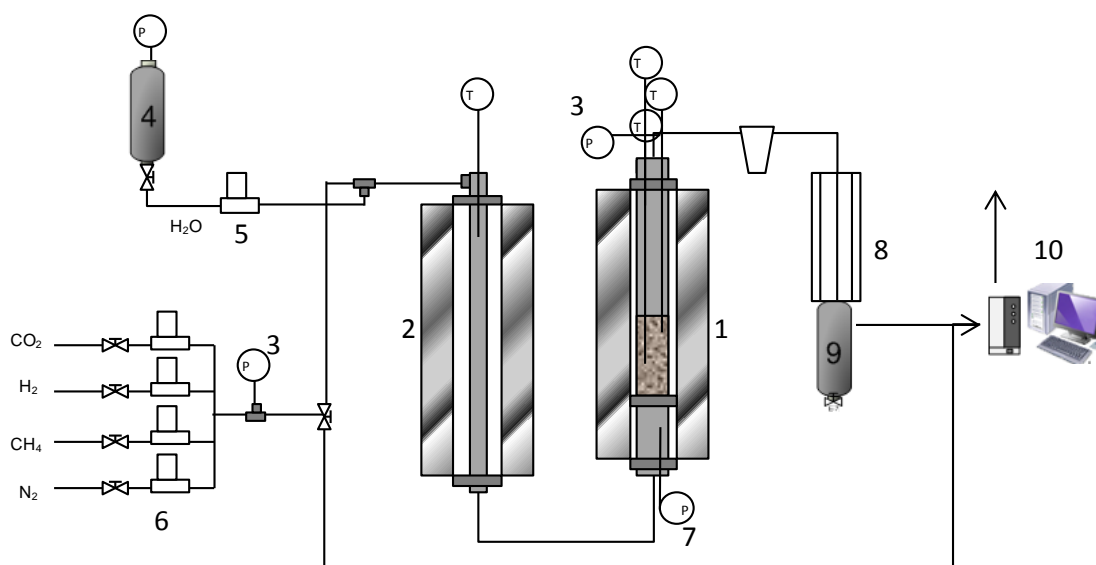
Figure 3 Fluidized bed reactor used at ICB-CSIC installations (1- Fluidized bed reactor, 2-Evaporator, 3-Manometer, 4-Pressurized water vessel, 5- Mass flow controller for liquids, 6-Mass flow controllers for gas, 8 and 9- water recovery system, 10-Online gas analyser and data acquisition system)

When performing the experiments with the 2p system, a total weight of 180 g of material was introduced into the reactor consisting of 135 g of calcined $CaO-Ca_{12}Al_{14}O_{33}$ sorbent and 45 g of reduced catalyst. Considering the composition of both materials given in Table 1, these quantities resulted in a CaO/Ni mass ratio of 6, and a total Ni content in bed of 3.75 wt%. To ensure that the gas velocity within the fluidized bed reactor was high enough to maintain proper fluidization of the particles within the solid bed, the minimum fluidization velocity was calculated. Considering the material properties shown in Table 1 and Table 2, a minimum fluidization velocity of 0.014 m/s for the sorbent particles in the 2p system was calculated using the values proposed by Wen and Yu (1966). The catalyst particles minimum fluidization velocity was slightly lower (i.e. 0.012 m/s) due to their lower particle size. Considering the minimum fluidization velocity for the sorbent particles in the 2p system, the superficial gas velocity used for the experiments performed with this particle system corresponded to a ratio between the superficial gas velocity and the minimum fluidization velocity between 4 and 7 that ensures proper fluidization conditions. For

9

the experiments carried out with the CCSM material, a total weight of 225 g of material was introduced into the reactor, in this case with the CaO/Ni mass ratio equal to 3 with a total Ni content in bed of 6 wt%. The minimum fluidization velocity for the CSCM particles was calculated according to the same procedure as for the 2p system, resulting in a value of 0.009 m/s. Table 3 and Table 4 give the experimental conditions for the tests performed for the 2p and 1p systems, respectively, in the rig depicted in Figure 3. The operation parameters analysed in the tests carried out were superficial gas velocity, steam-to-carbon molar ratio in the feed gas and CH_4 spatial velocity according to the amount of reduced catalyst in the solid bed (i.e. as $kg_{CH4}/h \cdot kg_{cat}$), linked to superficial gas velocity. The effect of these parameters on the product gas composition obtained at the reactor outlet during the different SER-regeneration cycles was evaluated in order to determine the operating window for the materials in this SER process. Temperature was kept constant and equal to 650 ºC during the SER stage for all the tests carried out in this work. It is important to highlight that all the tests indicated in Table 3 and Table 4 were performed using the same batch of solids in each case, and they were run sequentially, as indicated in these tables.

Table 3 Experimental conditions used for the SER tests performed in the fluidized bed reactor shown in Figure 3 for the 2-particle system

No.	Superficial gas velocity	S/C molar ratio	%H_2 in the mixture H_2-H_2O during regeneration	CH_4 space velocity [$kg_{CH4}/h \cdot kg_{cat}$]	No. Cycles
1	0.05	4	4	0.33	4
2	0.1	4	4	0.63	2
3	0.1	3	4	0.79	2
4	0.1	3	4	0.63	1
5	0.1	3	4	0.92	1
6	0.05	3	4	0.33	1
7	0.05	4	2	0.33	1
8	0.1	3	2	0.92	2

Table 4 Experimental conditions used for the SER tests performed in the fluidized bed reactor shown in Figure 3 for the 1-particle system

No.	Superficial gas velocity	S/C molar ratio	CH_4 volume flow rate [L_N/h]	CH_4 space velocity [$kg_{CH4}/h \cdot kg_{cat}$]	%CO_2 in the mixture CO_2-N_2 during regeneration	No. Cycles
1	0.05	4	21	0.17	50	3
2	0.05	3	21	0.17	50	1
3	0.1	4	40	0.33	50	1
4	0.1	3	40	0.33	50	1
5	0.1	4	40	0.33	60	2

The choice of regeneration conditions for the tests performed in the FBR comes from an extensive work performed within the ASCENT project (n.d.), which was aimed at maintaining the activity of the functional materials throughout cycling, as well as being representative for the process at

higher scale. Thus, for the 2p system, sorbent regeneration was performed in the presence of steam (wet regeneration stage) with a minimum content of H_2, to prevent oxidation of the catalyst particles due to the oxidising nature of the steam. An H_2 content of 4 vol% was used for most of the experiments performed in the FBR, since it has been demonstrated that this ensures proper catalyst performance. In order to evaluate the possibility of further reducing the consumption of H_2 in the regeneration stage, additional cycles were carried out where sorbent regeneration was performed including 2 vol% H_2 as indicated in Table 3. For the 1p system, the regeneration step was carried out at in 50 vol% CO_2 in N_2, since the presence of steam or the use of a pure CO_2 atmosphere during this stage were demonstrated to negatively impact the CO_2 sorption capacity of the CSCM material ("ASCENT project," n.d.). Also for this material, the effect of increasing CO_2 concentration during the regeneration was studied (see the Test No. 5 in Table 4) since this would allow reducing the CO_2-rich recycle needed in the regenerator reactor when operating such reactor in an O_2-rich atmosphere, boosting the overall efficiency of the process.

Table 5 and Table 6 summarize the experimental procedure followed for the tests with the 2p and 1p systems, respectively. In both tables, the procedure is detailed starting from the fresh material introduced into the FBR, and an initial pre-reduction period at high temperature is therefore included to ensure complete reduction of the catalyst. For the 1p system, the regeneration stage at 900 ℃ in CO_2/N_2 was also followed by a reduction period with 50 vol% H_2 in N_2 at the same temperature. For both particle systems, the cooling down from regeneration conditions to SER operating temperature was performed in an H_2/N_2 mixture with 5 vol% H_2.

Table 5 Experimental procedure followed in the FBR experiments for the 2-particle system

Step	$T_{initial}$ [℃]	T_{final} [℃]	Flow into the FBR	Gas composition of the gas fed to the FBR
Heating	25	400	36.5 L_N/h	100 vol% N_2
Heating in the presence of H_2	400	450	60 L_N/h	20 vol% H_2 in N_2
Heating in the presence of H_2 at a higher superficial gas velocity	450	850	100 L_N/h* 200 L_N/h**	20 vol% H_2 in N_2
Cooling period down to SER temperature	850	650	100 L_N/h* 200 L_N/h**	5 vol% H_2 95 vol% N_2
SER stage	650	650	120 L_N/h* 230 L_N/h**	Different compositions of $CH_4/H_2O/N_2$ depending on the S/C and CH_4 space velocity
Heating in the regeneration conditions	650	850	100 L_N/h*	4 vol% H_2 76 vol% H_2O 20 vol% N_2
			200 L_N/h**	4 vol% H_2 87 vol% H_2O 10 vol% N_2
Regeneration stage	850	850	100 L_N/h*	4 vol% H_2 76 vol% H_2O 20 vol% N_2

11

			200 L_N/h**	4 vol% H_2 87 vol% H_2O 10 vol% N_2

when performing SER stage with 0.05 m/s superficial velocity
when performing SER stage with 0.1 m/s superficial velocity

Table 6 Experimental procedure followed in the FBR experiments for the CSCM

Step	$T_{initial}$ [ºC]	T_{final} [ºC]	Flow into the FBR	Gas composition of the gas fed to the FBR
Heating	25	400	36.5 L_N/h	100 vol% N_2
Heating in the presence of H_2	400	850	70 L_N/h	50 vol% H_2 in N_2
Cooling period down to SER temperature	850	650	100 L_N/h* 200 L_N/h**	5 vol% H_2 95 vol% N_2
SER stage	650	650	120 L_N/h* 230 L_N/h**	Different compositions of CH_4/H_2O/N_2 depending on the S/C and CH_4 space velocity
Heating in the regeneration conditions	650	900	100 L_N/h* 200 L_N/h**	50 vol% CO_2 50 vol% N_2
Regeneration stage	900	900	100 L_N/h* 200 L_N/h**	50 vol% CO_2 50 vol% N_2
Reduction period	900	900	100 L_N/h* 200 L_N/h**	50 vol% H_2 in N_2

when performing SER stage with 0.05 m/s superficial velocity
when performing SER stage with 0.1 m/s superficial velocity

To evaluate the performance of the materials when testing different operating conditions, gas concentration profiles at the FBR outlet were compared with those obtained when equilibrium of reforming, WGS and CaO carbonation reactions was reached. Gas composition was evaluated referred to the gas free of H_2O and N_2, using the expression given in equation (4) where $X_{i,\text{free } H2O}$ corresponds to the concentration of the component i (i.e. H_2, CO, CO_2 and CH_4) measured by the online gas analyser placed downstream of the FBR (see Figure 3). $X_{N2,\text{free } H2O}$ in the same equation is the concentration of N_2 in the dry gas passing through the online analyser, calculated assuming that H_2, CO, CO_2 and CH_4 are the only components in the dry syngas sent to the analyser, being the remaining gas exclusively N_2.

$$X_{i,N2-H2O\,free} = \frac{X_{i,free\,H2O}}{1-X_{N2,free\,H2O}} \tag{4}$$

Equilibrium composition for a given temperature and S/C ratio was calculated using Aspen Hysys® software, considering the database for the reforming and WGS reactions and the equation of Baker (Baker, 1962) for the CaO carbonation reaction.

3. Results discussion

3.1. Operating limits for the 2p system in SER conditions

Figure 4 shows the evolution of a typical product gas concentration at the FBR outlet for SER test No.6 in Table 3 (i.e. S/C=3, 0.33 $kg_{CH4}/h \cdot kg_{cat}$ and 0.05 m/s superficial velocity). The dashed lines in this figure represent the calculated equilibrium composition for the experimental conditions tested. As shown in this figure, three different periods can be distinguished during the experiment (pre-, post- and breakthrough periods), which are typical of any reaction system operating in batch mode with a solid that is progressively converted, as is the case of the CO_2 sorbent here. At the beginning of the SER test (pre-breakthrough period), the $CaO-Ca_{12}Al_{14}O_{33}$ sorbent and the reforming catalyst are in calcined and reduced forms, respectively, and the CH_4 reforming, WGS and CaO carbonation reactions (Eqs.1-3) take place simultaneously in the reactor. Maximum H_2 concentration in the syngas produced is achieved during this period since the reforming and WGS reactions favour H_2 formation, enhanced by the separation of CO_2 from the gas phase by the carbonation of the CaO. When the CO_2 sorbent is fully carbonated and there is no longer any active CaO available in the solid bed, only CH_4 reforming and WGS take place, starting the post-breakthrough period. During the breakthrough period, the reaction between CO_2 and CaO reaches the diffusion regime and the CO_2 removal efficiency of the sorbent begins to decrease, resulting in reduced CH_4 conversion and H_2 concentration and an increase in the CO and CO_2 content, which eventually stabilizes during the post-breakthrough.
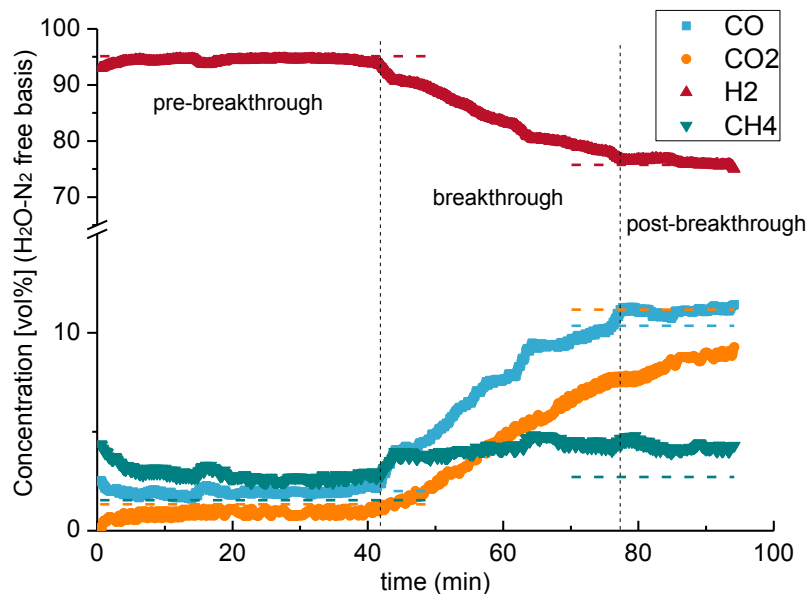
Figure 4 Evolution of gas concentration at the FBR outlet during the SER test carried out at 650 ºC with S/C=3, 0.33 $kg_{CH4}/h \cdot kg_{cat}$ and 0.05 m/s superficial velocity

As appreciated in Figure 4, the H_2, CO and CO_2 concentrations achieved at the FBR outlet during the pre-breakthrough period are close to the equilibrium for the conditions of S/C=3, 0.33 $kg_{CH4}/h \cdot kg_{cat}$ and 0.05 m/s superficial velocity. The CO_2 content in the syngas during the post-breakthrough period (i.e., indicated with orange dots in the figure) is shown to remain below the equilibrium concentration under these SMR conditions, increasing steadily towards the equilibrium value. This slow breakthrough is observed for the CO_2 concentration curve obtained for all tests carried out for the 2p and 1p systems in this work, which would indicate that there is still some residual carbonation of the CaO during this period that causes the CO_2 concentration to be below equilibrium value. The CH_4 concentration is seen to remain above the equilibrium values throughout the entire test (i.e. around 1.3% p.p. over the whole period). The formation of bubbles containing a fraction of the feed gas composed of CH_4, H_2O and N_2 is expected during the operation of the FBR, which would result in the by-pass of CH_4 from the inlet to the outlet of the reactor and therefore lead to CH_4 concentrations above equilibrium in the syngas. This slightly lower CH_4 conversion in SER processes operating in FBRs has been also observed within the scarce works published in the literature in this type of reactor (Arstad et al., 2012; Johnsen et al., 2006).

Carbon balance was solved in order to calculate the amount of CO_2 absorbed by the sorbent particles during the pre- and breakthrough periods. A CO_2 sorption capacity of around 0.27 g_{CO2}/g calcined sorbent (that expressed to the total bed weight amounts to 0.27 g_{CO2}/g bed material) was calculated for these periods, which was slightly higher than the sorption capacity of the individual sorbent particles tested in the TGA (Figure 2). The larger concentration of steam during the SER stage in this experiment (i.e. ≈53 %vol. H_2O in the feed gas) might be responsible for this increased sorption capacity since it improves the CO_2 diffusion through the product layer, as already observed by other authors in the literature (García-Lario et al., 2015b).

Once the typical concentration profile at the FBR outlet has been described, the operating limits for the 2p system under SER conditions have been assessed. These operating limits have been defined in terms of the maximum CH_4 space velocity that can be processed for the sorbent-to-catalyst mass ratio of 3 at two different S/C molar ratios (3 and 4). When working above the maximum CH_4 space velocity, two situations could occur during the pre-breakthrough period: (i) the sorbent cannot react with CO_2 as fast as it is produced by the reforming and WGS reactions, thus CO accumulates in the gas phase and H_2 does not reach equilibrium; and/or (ii) the reforming catalyst has low activity for such high CH_4 space velocity and cannot process all the CH_4 entering the reactor, resulting again in a lower H_2 concentration than equilibrium and a higher CH_4 content. In the latter case, the H_2 content in the gas phase would also be lower than equilibrium during the post-breakthrough period, when only reforming and WGS reactions are occurring.

To determine the effect that the S/C molar ratio might have on the operating limits of the system, the results for the experiments carried out with different S/C ratios maintaining the superficial

velocity at 0.1 m/s and the CH_4 space velocity at 0.63 kg_{CH4}/h kg_{cat} have been plotted in Figure 5. As shown, for the experiment with S/C=4 the H_2, CO and CO_2 contents at the FBR outlet correspond to those values at equilibrium during the SER period. H_2 concentrations close to 96 vol% (H_2O-N_2 free) were reached for these conditions, while the CO_2 content stabilized at 0.8 vol% (H_2O-N_2 free). However, SER equilibrium was not reached with the S/C ratio of 3; this was particularly clear for the H_2 content and CH_4, which reached a stable value of close to 4.2 vol % (dry basis and free of N_2), noticeably high when compared to the value of around 2 vol% reached for S/C=4. Considering the CH_4 content at equilibrium conditions for both experiments (i.e. 1.9 vol% for S/C=3 and 0.5 vol% for S/C=4, both given as H_2O-N_2 free), it is evident that the difference between the CH_4 content at the FBR outlet and the equilibrium value is raised by 50% for S/C=3, which indicates that the CH_4 is being accumulated in the gas phase. Moreover, CO content during the pre-breakthrough period stabilizes at around 1 percentage point above the CO equilibrium value of 1.3 vol% (H_2O-N_2 free) for these conditions. To elucidate which is the limiting material within the pre-breakthrough it is necessary to evaluate the performance of the system once the sorbent is saturated in the post-breakthrough.

Looking into the gas composition during the post-breakthrough for the curve with S/C=3 in Figure 5, the H_2 content in the syngas at the FBR outlet matched the equilibrium value, indicating that the performance of the Ni-based catalyst is not limited by the operating conditions of larger CH_4 spatial velocity and superficial velocity. Therefore, the operating limits of the CaO-$Ca_{12}Al_{14}O_{33}$ sorbent might be close to S/C=3, 0.1 m/s superficial velocity and 0.63 kg_{CH4}/h·kg_{cat} of CH_4 spatial velocity, as it is not able to process the CO_2 as fast as it is formed by the reforming and WGS reactions, and so causing the accumulation of CO and CH_4 observed during the SER period.
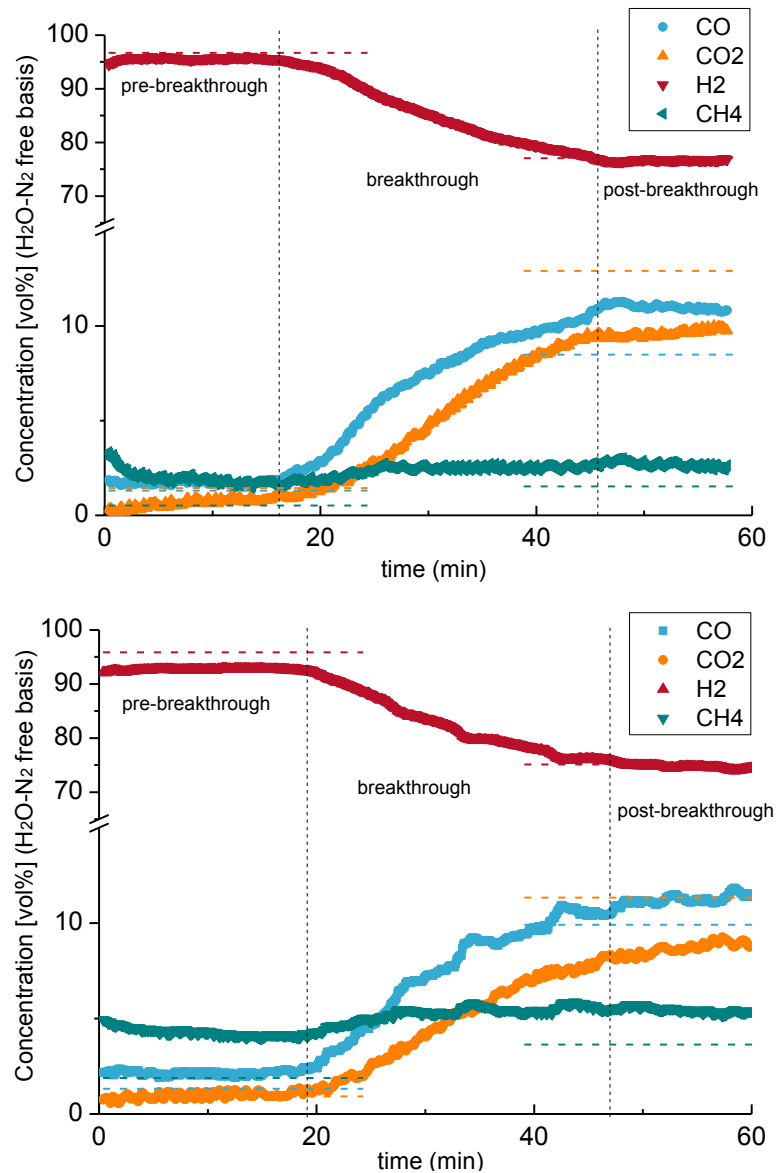
Figure 5 Evolution of gas concentration at the FBR outlet during the SER test carried out at 650 °C with 0.63 kg$_{CH4}$/h·kg$_{cat}$ and 0.10 m/s superficial velocity for different S/C ratios: S/C=4 (top) and S/C=3 (bottom)

Once the operation limit for the CaO-Ca$_{12}$Al$_{14}$O$_{33}$ sorbent was determined, the performance of the 2p system was assessed when modifying the CH$_4$ spatial velocity in the FBR in order to elucidate the operating limit of the Ni/MgAl$_2$O$_4$ catalyst. Table 7 summarizes the average H$_2$ and CH$_4$ contents measured at the FBR outlet during the pre- and post-breakthrough periods when modifying the CH$_4$ spatial velocity from 0.63 to 0.92 kg$_{CH4}$/h·kg$_{cat}$ for the S/C ratio of 3 and the superficial gas velocity of 0.1 m/s. Equilibrium contents of H$_2$ and CH$_4$ for such conditions correspond to 95.3-95.9 vol% (H$_2$O-N$_2$ free) and 75 vol%. (H$_2$O-N$_2$ free) for the SER and SMR periods, respectively. As shown in this table, the H$_2$ content at the syngas outlet remains at the same value of 92.6 vol% during the SER period for the CH$_4$ spatial velocities of 0.63 and 0.79 kg$_{CH4}$/h·kg$_{cat}$, and it decreases appreciably as the spatial velocity rises to 0.92 kg$_{CH4}$/h·kg$_{cat}$. For

the latter spatial velocity, the H_2 equilibrium during SMR is no longer reached, being stabilized at around 2 percentage points below the equilibrium value. Based on these results, for the sorbent-to-catalyst weight ratio of 3 used in the FBR (i.e. 3.75 wt% Ni content in the solid bed), it can be concluded that the Ni-based catalyst used cannot perform properly when working with CH_4 spatial velocities of 0.92 $kg_{CH4}/h \cdot kg_{cat}$, having shown instead adequate kinetics towards SMR for a spatial velocity of 0.79 $kg_{CH4}/h \cdot kg_{cat}$ and an S/C ratio of 3.

Table 7 Average H_2 and CH_4 concentration values during the pre- and post-breakthrough periods at the FBR outlet for 2p-system tests carried out with S/C=3 and superifical velocity of 0.1 m/s for different CH_4 spatial velocities (standard deviation is indicated in brackets)
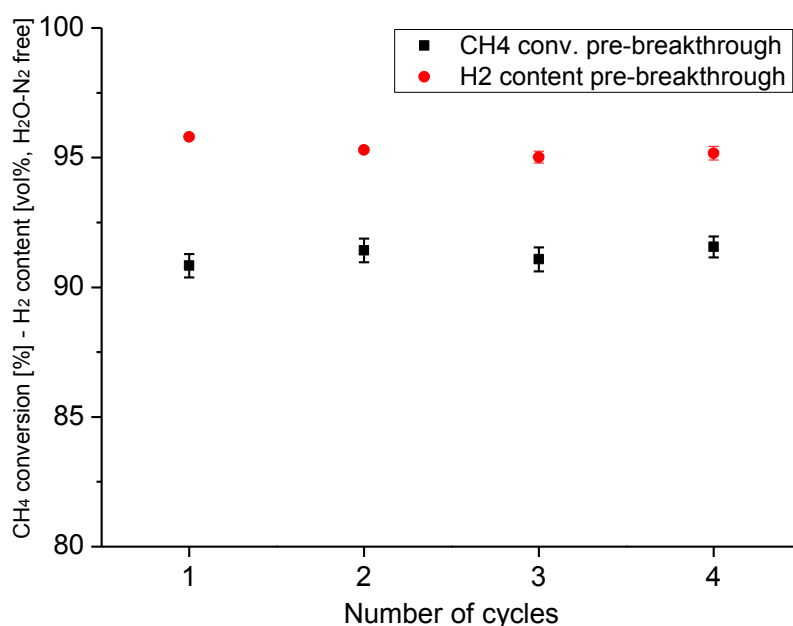
CH₄ spatial velocity [kg$_{CH4}$/h·kg$_{cat}$]	H₂ content in the syngas [vol%] (H₂O-N₂ free)		CH₄ content in the syngas [vol%] (H₂O-N₂ free)	
	Pre-breakthrough	Post-breakthrough	Pre-breakthrough	Post-breakthrough
0.63	92.6 (0.16)	74.3 (0.26)	4.3 (0.21)	5.4 (0.08)
0.79	92.6 (0.21)	74.8 (0.36)	4.3 (0.32)	4.9 (0.06)
0.92	91.3 (0.11)	72.9 (0.07)	6.1 (0.22)	7.0 (0.05)

Figure 6 shows the reproducibility of performance for the results obtained during 4 consecutive SER-regeneration cycles for the 2p system using an S/C ratio of 4, 0.33 kg_{CH4}/h kg_{cat} and 0.05 m/s superficial gas velocity during SER stage. CH_4 conversion indicated in this figure was calculated as the average of the individual CH_4 conversion values ($X_{CH4,t}$) calculated during the pre- and post-breakthrough periods according to equation (5). In this equation, $\dot{N}_{CH4,in}$ corresponds to the flow rate of CH_4 introduced into the FBR and $\dot{N}_{CH4,out(t)}$ to the flow rate of CH_4 in the syngas at a given time t, which is estimated with the gas composition and the syngas flow rate at the reactor outlet.

$$X_{CH4,t} = \frac{\dot{N}_{CH4,in} - \dot{N}_{CH4,out\ (t)}}{\dot{N}_{CH4,in}} \tag{5}$$

As shown in Figure 6, the performance of the 2p system was maintained throughout consecutive experiments, reaching H_2 contents of 95-95.8 vol% (H₂O-N₂ free) during the SER period, very close to the H_2 content at equilibrium conditions. CH_4 conversion calculated during the same period was in the range of 91–91.6 % for the different cycles. Regarding the sorption capacity of the sorbent particles, it was estimated through the mass balances of Test No.1, indicated in Table 3, that the CO_2 sorption capacity would slightly decrease from 0.25 g_{CO2}/g calcined sorbent to 0.23 g_{CO2}/g calcined sorbent during the three following cycles, in agreement with the results obtained in the TGA. However, from this cycle onwards (i.e. from Test No.2 to No.8) this CO_2

sorption capacity was observed to slightly increase over 0.25 g_{CO_2}/g calcined sorbent, proving the stability of the material.

Figure 6 CH_4 conversion and H_2 content in the syngas during the pre-breakthrough period (left axis) in the 2p system during 4 consecutive SER-regeneration cycles (S/C=4, 0.33 kg_{CH4}/h·kg_{cat} and 0.05 m/s superficial velocity for the SER stage)

Finally, once the operating window for the materials tested was determined, the possibility of reducing the amount of H_2 introduced during the regeneration stage was assessed. As anticipated, reducing the consumption of H_2 during the regeneration of the sorbent would have a positive impact on the overall performance of the system. However, if not enough H_2 were introduced into the regenerator, the catalyst particles could be oxidized and (partly) deactivated. To assess this effect, three consecutive cycles were carried out, pushing the catalyst to work under stringent conditions (i.e. at a CH_4 spatial velocity of 0.92 kg CH_4/h kg cat and an S/C of 3), but performing the regeneration of the sorbent in a rich steam stream that contained only 2 vol% H_2/vol. H_2O. Figure 7 shows the H_2 and CH_4 concentration profiles obtained at the FBR outlet for such experiments. As appreciated, the H_2 content of the syngas obtained progressively decreases during the cycles, with a reduction of 1.7 percentage points between first and second cycles and around 1.3 percentage points from the second to the third cycle, and contrary to the trend shown for the CH_4, which accumulates in the syngas with the cycles. Based on this figure, it can be concluded that regenerating the 2p system with only 2 vol% H_2 in steam is not sufficient to keep up the activity of the catalyst during cycling. As mentioned before, XRD analysis was made to the solids extracted from the FBR at the end of the tests included in Table 3. The objective of this analysis was determining if there were any interaction between the phases during the experimental tests. For the CO_2 sorbent material, $CaCO_3$, CaO and $Ca_{12}Al_{14}O_{33}$ were the only crystalline species

18

present in the XRD pattern, which confirms the absence of any interaction between them. $CaCO_3$ was present in the XRD diffractogram since the material was extracted from the reactor without being calcined. As for the commercial catalyst, Ni and $MgAl_2O_4$ corresponded to the main crystalline phases detected, as for the fresh catalyst particles in agreement with the results presented by Di Felice et al. (2019) after long testing in TGA.
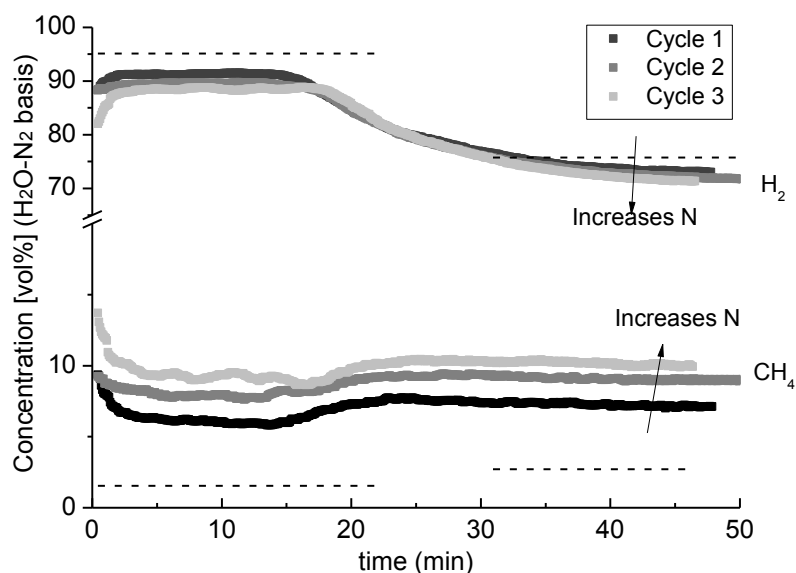

Figure 7 H_2 and CH_4 concentration during three consecutive SER experiments with S/C=3 and 0.92 $kg_{CH4}/h \cdot kg_{cat}$ including an intermediate regeneration step at 850 ºC under an atmosphere of 2 vol% H_2 in steam (the growing number of cycles is indicated by lightening the coloured lines)

Summarizing the results obtained for the 2p system, the mixture of the $CaO-Ca_{12}Al_{14}O_{33}$ sorbent and the $Ni/MgAl_2O_4$ catalyst particles has demonstrated an ability to convert up to 0.63 $kg_{CH4}/h \cdot kg_{cat}$ for a solid bed containing as low as 3.75 wt% Ni, at a superficial gas velocity of 0.1 m/s and an S/C ratio of 4. These S/C conditions have demonstrated to be those that maximize the H_2 production efficiency of the SER process according to thermodynamics. However, when seeking the conditions to maximize the efficiency of a hydrogen production plant based on this process (i.e. accounting for electricity consumption and the excess of steam to be exported from the plant), lower S/C ratios would be desirable in order to benefit from the credits obtained when using lower amounts of steam inside the SER reactor (Martínez et al., 2013). In this case, the CH_4 introduced into the FBR should be decreased to 0.33 $kg_{CH4}/h \cdot kg_{cat}$ to ensure a proper performance of this sorbent/catalyst system. Working with larger CH_4 inputs would be possible by increasing the amount of sorbent in the solid bed (i.e. reducing the % of Ni as long as the operating limits of the catalyst are not exceeded) to ensure that there is enough active CaO available to react with the CO_2 produced. Regarding the regeneration conditions for the material system, a minimum concentration of 4 vol% H_2 is needed to prevent the deactivation of the catalyst owing to oxidation by steam.

3.2. CSCM performance

The results obtained for the CSCM material are discussed in this section. The main advantage of using a combined material when scaling SER technology lies in the possibility of reducing the amount of inert material present in the fluidized bed reactor, which acts as a thermal ballast for the process by absorbing part of the energy released within the SER reactor that cannot be ultimately recovered. Moreover, particle segregation within the solid bed is avoided and the loss of material in the form of fines would be homogenous, facilitating the reprocessing of collected material. The combined material used in this work was prepared by mechanically mixing the individual functional materials used in the 2p system, as described in the materials preparation section, which resulted in an inert content that was not reduced with respect to the solid bed in the 2psystem. However, there is still a lot of ongoing work on the optimization of these combined materials with regard to their composition and performance during cycles under different conditions (Di Giuliano and Gallucci, 2018), and the testing of any of these still immature materials was outside of the scope of this work. The objective of the tests carried out in the laboratory-scale FBR was therefore to demonstrate that the combined material prepared can at least give the same performance as the separate functional materials.

Figure 8 shows the evolution of the gas concentration at the FBR outlet for a CH_4 spatial velocity of 0.17 kg_{CH4}/h·kg_{cat} for the two different S/C ratios of 3 and 4. Equilibrium was reached for both S/C ratios during both the pre- and post-breakthrough periods. H_2 concentrations up to 96 vol% (H_2O-N_2 free basis) were achieved at SER conditions for an S/C ratio of 4, which dropped to 77 vol% during the post-breakthrough period, when only reforming and WGS reactions were occurring. For the test performed at an S/C of 3, up to 94.5 vol% H_2 was obtained during the pre-breakthrough period, and 77 vol% once the sorbent function in the CSCM was saturated. Despite the differences in the S/C ratio, the duration of the pre-breakthrough period is not altered and it takes around 30 min before the breakthrough period starts. A CSCM CO_2 sorption capacity of around 0.14 g_{CO2}/g_{CSCM} (considering the CSCM weight as fully calcined and reduced) has been calculated through the C balance over the periods where CO_2 is being absorbed (i.e. pre- and breakthrough periods). Considering the weight of granulated CaO-$Ca_{12}Al_{14}O_{33}$ sorbent that was used for preparing such combined material, this CO_2 sorption capacity is equivalent to 0.23 g_{CO2}/g calcined sorbent, which was the conversion observed in the TGA (Figure 2), demonstrating that sorbent performance is maintained after the granulation process with the commercial catalyst particles.

20
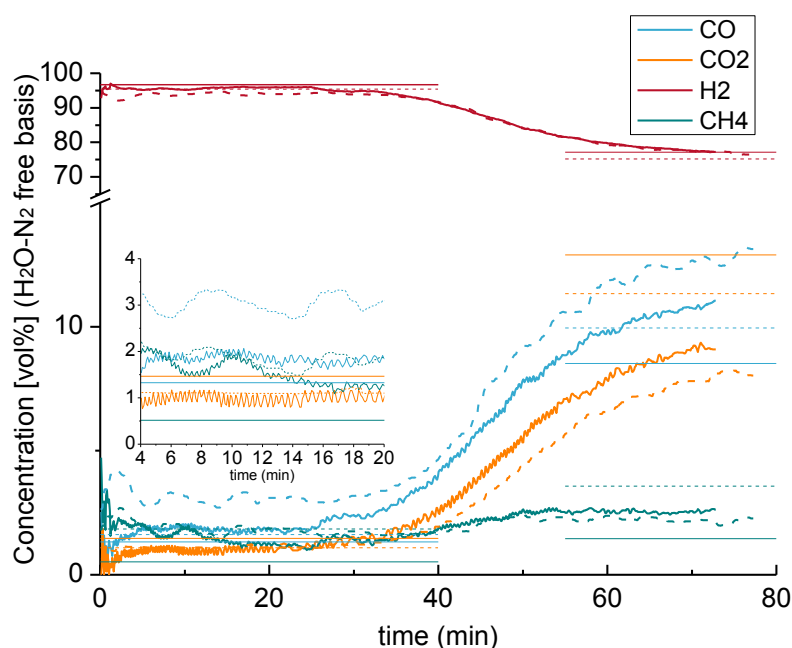
Figure 8 Evolution of gas concentration at the FBR outlet obtained for the CSCM at 650 ºC with 0.17 kg$_{CH4}$/h·kg$_{cat}$ and 0.05 m/s superficial velocity for an S/C=3 (dashed lines) and S/C=4 (continuous lines) (cycle 2). Regeneration performed at 900 ºC in 50 vol% CO$_2$/N$_2$. Straight lines represent equilibrium values for S/C=3 (dashed lines) and S/C=4 (continuous lines)

With regard to the effect of the CH$_4$ spatial velocity on CSCM performance, Figure 9 shows the gas concentration profiles obtained for an S/C ratio of 4 for the two spatial velocities of 0.17 kg$_{CH4}$/h·kg$_{cat}$ and 0.3 kg$_{CH4}$/h·kg$_{cat}$. Higher spatial velocities such as those used in the 2p system were not possible in the FBR used in this work with the CSCM since they would result in very large gas superficial velocities (i.e. >0.18 m/s to achieve 0.63 kg$_{CH4}$/h·kg$_{cat}$), which would result in the elutriation of the material from the solid bed. As shown by the results plotted in Figure 9, the CSCM maintains its good performance for the higher spatial velocity of 0.3 kg$_{CH4}$/h·kg$_{cat}$, reaching the same H$_2$ concentration of close to 96 vol% (H$_2$O-N$_2$ free) during the pre-breakthrough period as for the lower spatial velocity. The only effect of working with a doubled flow of CH$_4$ into the FBR is the duration of the pre-breakthrough period, which is halved, as shown in this figure. An additional test was performed maintaining the CH$_4$ spatial velocity at 0.3 kg$_{CH4}$/h·kg$_{cat}$ but reducing the S/C ratio to 3 (Test No.4 in Table 4). The results indicated that the CSCM was also able to reach equilibrium composition under these conditions.
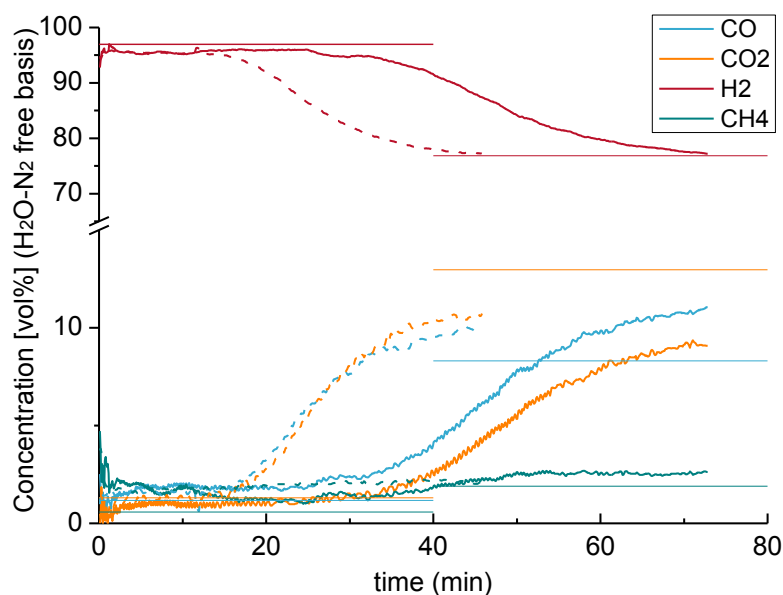
Figure 9 Evolution of gas concentration at the FBR outlet obtained for the CSCM at 650 ºC with S/C=4 using two different gas and CH$_4$ spatial velocities: 0.17 kg$_{CH4}$/h·kg$_{cat}$ and 0.05 m/s superficial gas velocity (continuous lines) and 0.33 kg$_{CH4}$/h·kg$_{cat}$ and 0.1 m/s superficial gas velocity (dashed lines). Regeneration performed at 900 ºC in 50 vol% CO$_2$/N$_2$

Finally, the impact of the regeneration conditions was assessed by performing two additional cycles with a regeneration step at 925 ºC and 60 vol% CO$_2$ in N$_2$. Figure 10 shows the results obtained for two consecutive SER experiments performed after a regeneration step under such conditions. As shown in this figure, these harsher conditions during regeneration did not affect the performance of the CSCM during the SER tests. The H$_2$ concentration reached the equilibrium value of almost 96 vol% (in H$_2$O-N$_2$ free basis) and the CO$_2$ sorption capacity remained unaltered at around 0.14 g$_{CO2}$/g$_{CSCM}$ throughout these cycles. XRD analysis of the CSCM extracted from the FBR after the tests indicated that no new mixed phases were formed between the sorbent and catalyst phases in the CSCM, being Ca$_{12}$Al$_{14}$O$_{33}$, CaCO$_3$, MgAl$_2$O$_4$, MgO, Ni, Al$_2$O$_3$ and CaO the species present, in agreement with the results from Di Felice et al. (2019). These promising results confirm the suitability of this combined material for the dual fluidized bed SER process, where regeneration of the sorbent is carried out in the presence of large CO$_2$ concentrations, but in the absence of O$_2$ to prevent the deactivation of the material ("ASCENT project," n.d.).
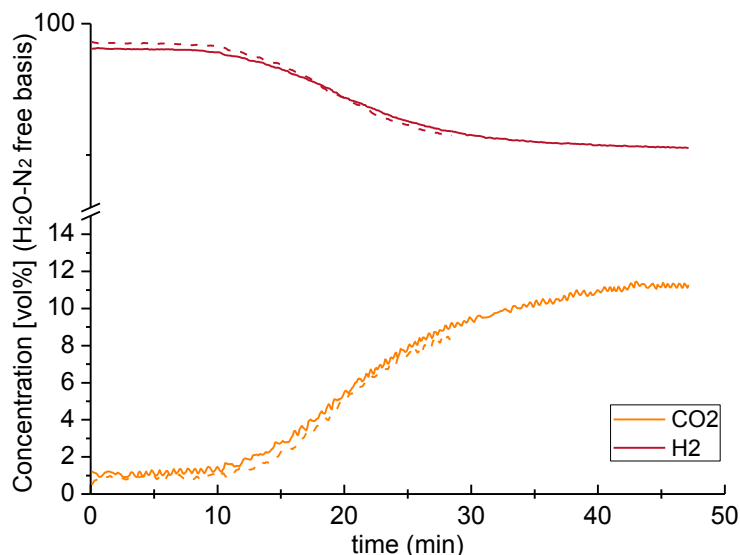
Figure 10 H_2 and CO_2 concentrations during two consecutive SER experiments with S/C=4 and 0.3 $kg_{CH4}/h \cdot kg_{cat}$ performed after a regeneration step at 925 ºC in 60 vol% CO_2 in N_2 (continuous lines refer to first cycle and dashed lines to the second cycle)

4. Conclusions

A synthetic $CaO-Ca_{12}Al_{14}O_{33}$ CO_2 sorbent prepared following a hydrothermal synthesis route has been successfully tested in a FBR in consecutive SER/regeneration cycles. The performance and operating limits of this sorbent and a reforming catalyst mixture were assessed in the FBR under relevant SER operating conditions. H_2 contents as high as 96 vol% (N_2 free, dry basis) were achieved under SER operation using these materials with a sorbent-to-catalyst weight ratio of 3 (i.e. 3.75 wt% Ni content in the solid bed) at 650 ºC with S/C ratios of 3 and 4. This solid system is able to convert up to 0.63 $kg_{CH4}/h \cdot kg_{cat}$ at a superficial gas velocity of 0.1 m/s and an S/C ratio of 4, requiring the reduction of the CH_4 input to 0.33 $kg_{CH4}/h \cdot kg_{cat}$ when working with a lower S/C ratio. The $CaO-Ca_{12}Al_{14}O_{33}$ sorbent presented a stable CO_2 sorption capacity of around 0.25 g_{CO2}/g calcined sorbent throughout the SER/regeneration cycles, which corresponds to 0.19 g_{CO2}/g bed material. Focusing on the regeneration conditions for this 2-particle system, it has been experimentally observed that a minimum concentration of 4 vol% H_2 is needed in the calciner to prevent the deactivation of the catalyst due to oxidation.

Moreover, a CSCM was successfully tested in consecutive SER/regeneration cycles in the FBR. Similar H_2 contents as for the separated materials were obtained with the CSCM working with 0.33 $kg_{CH4}/h \cdot kg_{cat}$ at 0.1 m/s superficial gas velocity and S/C ratios of 3 and 4. The CO_2 sorption capacity of the combined material was the same as that of the separate sorbent particles, corresponding to 0.14 g_{CO2}/g_{CSCM}. CSCM regeneration was performed in a CO_2-rich atmosphere (i.e. 50 vol%) and at a higher temperature than for the 2-particle system (i.e. 900 ºC). The effect of increased CO_2 content and temperature under regeneration was evaluated and no evident negative impact was observed on material performance.

Acknowledgements

References

Abanades, J.C., Murillo, R., Fernández, J.R., Grasa, G., Martínez, I., 2010. New CO2 capture process for hydrogen production combining Ca and Cu chemical loops. Environ. Sci. Technol. 44, 6901–6904. doi:10.1021/es101707t

Aloisi, I., Di Giuliano, A., Di Carlo, A., Foscolo, P.U., Courson, C., Gallucci, K., 2017. Sorption enhanced catalytic Steam Methane Reforming: Experimental data and simulations describing the behaviour of bi-functional particles. Chem. Eng. J. 314, 570–582. doi:10.1016/j.cej.2016.12.014

Antzara, A., Heracleous, E., Bukur, D.B., Lemonidou, A.A., 2015. Thermodynamic analysis of hydrogen production via chemical looping steam methane reforming coupled with in situ CO2 capture. Int. J. Greenh. Gas Control 32, 115–128. doi:10.1016/j.ijggc.2014.11.010

Arstad, B., Blom, R., Bakken, E., Dahl, I., Jakobsen, J.P., Røkke, P., 2009. Sorption-enhanced methane steam reforming in a circulating fluidized bed reactor system, in: Energy Procedia. pp. 715–720. doi:10.1016/j.egypro.2009.01.094

Arstad, B., Prostak, J., Blom, R., 2012. Continuous hydrogen production by sorption enhanced steam methane reforming (SE-SMR) in a circulating fluidized bed reactor: Sorbent to catalyst ratio dependencies. Chem. Eng. J. 189–190, 413–421. doi:10.1016/j.cej.2012.02.057

ASCENT project [WWW Document], n.d. URL http://ascentproject.eu (accessed 6.13.18).

Baker, E.H., 1962. The CaO-CO2 system in the pressure range 1-300 atm. J. Chem. Soc. 70, 464–470.

Cesário, M.R., Barros, B.S., Courson, C., Melo, D.M.A., Kiennemann, A., 2015. Catalytic performances of Ni–CaO–mayenite in CO2 sorption enhanced steam methane reforming. Fuel Process. Technol. 131, 247–253. doi:10.1016/j.fuproc.2014.11.028

Chanburanasiri, N., Ribeiro, A.M., Rodrigues, A.E., Arpornwichanop, A., Laosiripojana, N., Praserthdam, P., Assabumrungrat, S., 2011. Hydrogen production via sorption enhanced steam methane reforming process using Ni/CaO multifunctional catalyst. Ind. Eng. Chem. Res. 50, 13662–13671. doi:10.1021/ie201226j

Di Felice, L., Kazi, S.S., Sørby, M.H., Martínez, I., Grasa, G., Maury, D., Meyer, J., 2019. Combined sorbent and catalyst material for sorption enhanced reforming of methane under cyclic regeneration in presence of H2O and CO2. Fuel Process. Technol. 183, 35–47. doi:https://doi.org/10.1016/j.fuproc.2018.10.012

Di Giuliano, A., Gallucci, K., 2018. Sorption enhanced steam methane reforming based on nickel and calcium looping: a review. Chem. Eng. Process. - Process Intensif. 130, 240–252. doi:10.1016/J.CEP.2018.06.021

Di Giuliano, A., Girr, J., Massacesi, R., Gallucci, K., Courson, C., 2017. Sorption enhanced steam methane reforming by Ni–CaO materials supported on mayenite. Int. J. Hydrogen

Energy 42, 13661–13680. doi:10.1016/J.IJHYDENE.2016.11.198

Edenhofer, O., Pichs-Madruga, R., Sokona, Y., Farahani, E., Kadner, S., Seyboth, K., Adler, A., Baum, I., Brunner, S., Eickemeier, P., Kriemann, B., Savolaninen, J., 2014. IPCC, 2014: Climate Change 2014: Mitigation of Climate Change. Contribution of Working Group III to the Fifth Assessment Report of the Intergovernmental Panel on Climate Change. Cambridge University Press, Cambridge, United Kingdom and New York, NY, USA.

Erans, M., Manovic, V., Anthony, E.J., 2016. Calcium looping sorbents for CO2 capture. Appl. Energy 180, 722–742. doi:10.1016/J.APENERGY.2016.07.074

Fernández, J.R., Abanades, J.C., Grasa, G., 2012. Modeling of sorption enhanced steam methane reforming—Part II: Simulation within a novel Ca/Cu chemical loop process for hydrogen production. Chem. Eng. Sci. 84, 12–20. doi:http://dx.doi.org/10.1016/j.ces.2012.07.050

García-Lario, A.L., Aznar, M., Grasa, G.S., Murillo, R., 2015a. Evaluation of process variables on the performance of Sorption Enhanced Methane Reforming. J. Power Sources 285, 90–99. doi:10.1016/J.JPOWSOUR.2015.03.075

García-Lario, A.L., Aznar, M., Martínez, I., Grasa, G.S., Murillo, R., 2015b. Experimental study of the application of a NiO/NiAl2O4 catalyst and a CaO-based synthetic sorbent on the Sorption Enhanced Reforming process. Int. J. Hydrogen Energy 40, 219–232. doi:10.1016/j.ijhydene.2014.10.033

García-Lario, A.L., Grasa, G.S., Murillo, R., 2015c. Performance of a combined CaO-based sorbent and catalyst on H2 production, via sorption enhanced methane steam reforming. Chem. Eng. J. 264, 697–705. doi:10.1016/J.CEJ.2014.11.116

Grasa, G.S., Abanades, J.C., 2006. CO2 Capture Capacity of CaO in Long Series of Carbonation/Calcination Cycles. Ind. Eng. Chem. Res. 45, 8846–8851.

Han, C., Harrison, D.P., 1994. Simultaneous shift reaction and carbon dioxide separation for the direct production of hydrogen. Chem. Eng. Sci. doi:10.1016/0009-2509(94)00266-5

Harrison, D.P., 2008. Sorption-enhanced hydrogen production: A review. Ind. Eng. Chem. Res. 47, 6486–6501. doi:10.1021/ie800298z [doi]

Hildenbrand, N., Readman, J., Dahl, I.M., Blom, R., 2006. Sorbent enhanced steam reforming (SESR) of methane using dolomite as internal carbon dioxide absorbent: Limitations due to Ca(OH)2formation. Appl. Catal. A Gen. 303, 131–137. doi:10.1016/j.apcata.2006.02.015

IEA, 2006. Hydrogen Production and Storage. R&D Priorities and Gaps. doi:10.1016/0360-3199(88)90106-1

Johnsen, K., Ryu, H.J., Grace, J.R., Lim, C.J., 2006. Sorption-enhanced steam reforming of methane in a fluidized bed reactor with dolomite as CO2-acceptor. Chem. Eng. Sci. 61, 1195–1202. doi:10.1016/j.ces.2005.08.022

Kalantzopoulos, G., Kazi, S., Grasa, G., Mastin, J., Murillo, R., Meyer, J., 2015. Development of high performance CO2 solid sorbents combined with a reforming catalyst for hydrogen production by Sorption-Enhanced Reforming (SER), in: Proceedings of the Energy & Materials Research (EMR) Conference. BrownWalker Press.

Kazi, S.S., Aranda, A., Meyer, J., Mastin, J., 2014. High performance CaO-based sorbents for pre- and post- combustion CO2 capture at high temperature. Energy Procedia 63, 2207–2215. doi:10.1016/J.EGYPRO.2014.11.240

Li, Z.S., Cai, N.S., Huang, Y.Y., 2006a. Effect of preparation temperature on cyclic CO2 capture and multiple carbonation-calcination cycles for a new Ca-based CO2 sorbent. Ind. Eng. Chem. Res. 45, 1911–1917. doi:10.1021/ie0512111

Li, Z.S., Cai, N.S., Yang, J.B., 2006b. Continuous production of hydrogen from sorption-enhanced steam methane reforming in two parallel fixed-bed reactors operated in a cyclic manner. Ind. Eng. Chem. Res. 45, 8788–8793. doi:10.1021/ie061010x

López, J.M., Grasa, G., Murillo, R., 2018. Evaluation of the effect of inert support on the carbonation reaction of synthetic CaO-based CO2 sorbents. Chem. Eng. J. 350, 559–572. doi:10.1016/J.CEJ.2018.05.014

Lopez Ortiz, A., Harrison, D.P., 2001. Hydrogen Production Using Sorption-Enhanced Reaction. Ind. Eng. Chem. Res. 40, 5102–5109. doi:10.1021/ie001009c

Martavaltzi, C.S., Lemonidou, A.A., 2010. Hydrogen production via sorption enhanced reforming of methane: Development of a novel hybrid material-reforming catalyst and CO2 sorbent. Chem. Eng. Sci. 65, 4134–4140. doi:10.1016/j.ces.2010.04.038

Martavaltzi, C.S., Pefkos, T.D., Lemonidou, A.A., 2011. Operational window of sorption enhanced steam reforming of methane over CaO-Ca12Al14O33. Ind. Eng. Chem. Res. 50, 539–545. doi:10.1021/ie1002284

Martínez, I., Romano, M.C., Chiesa, P., Grasa, G., Murillo, R., 2013. Hydrogen production through sorption enhanced steam reforming of natural gas: Thermodynamic plant assessment. Int. J. Hydrogen Energy 38, 15180–15199. doi:10.1016/j.ijhydene.2013.09.062

Mastin, J., Aranda, A., Meyer, J., 2011. New synthesis method for CaO-based synthetic sorbents with enhanced properties for high-temperature CO2-capture. Energy Procedia 4, 1184–1191. doi:10.1016/j.egypro.2011.01.172

Meyer, J., Mastin, J., Bjørnebøle, T.K., Ryberg, T., Eldrup, N., 2011. Techno-economical study of the Zero Emission Gas power concept, in: Energy Procedia. pp. 1949–1956. doi:10.1016/j.egypro.2011.02.075

Ochoa-Fernandez, E., Haugen, G., Zhao, T., Ronning, M., Aartun, I., Borresen, B., Rytter, E., Ronnekleiv, M., Chen, D., 2007. Process design simulation of H2 production by sorption enhanced steam methane reforming: evaluation of potential CO2 acceptors. Green Chem.

doi:10.1039/b614270b

Romano, M.C., Cassotti, E.N., Chiesa, P., Meyer, J., Mastin, J., 2011. Application of the Sorption Enhanced-Steam Reforming process in combined cycle-based power plants, in: Energy Procedia. pp. 1125–1132. doi:10.1016/j.egypro.2011.01.164

Shokrollahi Yancheshmeh, M., Radfarnia, H.R., Iliuta, M.C., 2016. High temperature CO_2 sorbents and their application for hydrogen production by sorption enhanced steam reforming process. Chem. Eng. J. 283, 420–444. doi:10.1016/j.cej.2015.06.060

Waldron, W.E., Hufton, J.R., Sircar, S., 2001. Production of hydrogen by cyclic sorption enhanced reaction process. AIChE J. 47, 1477–1479. doi:doi.org/10.1002/aic.690470623

Wen, C.Y., Yu, Y.H., 1966. A generalized method for predicting the minimum fluidization velocity. AIChE J. 12, 610–612. doi:10.1002/aic.690120343

Yi, K.B., Harrison, D.P., 2005. Low-pressure sorption-enhanced hydrogen production. Ind. Eng. Chem. Res. 44, 1665–1669. doi:10.1021/ie048883g

Yin, J., Qin, C., An, H., Liu, W., Feng, B., 2012. High-Temperature Pressure Swing Adsorption Process for CO_2 Separation. Energy & Fuels 26, 169–175. doi:10.1021/ef201142w

Zamboni, I., Zimmermann, Y., Kiennemann, A., Courson, C., 2015. Improvement of steam reforming of toluene by CO_2 capture using $Fe/CaO–Ca_{12}Al_{14}O_{33}$ bi-functional materials. Int. J. Hydrogen Energy 40, 5297–5304. doi:10.1016/j.ijhydene.2015.01.065

Zhu, L., Fan, J., 2015. Thermodynamic analysis of H_2 production from CaO sorption-enhanced methane steam reforming thermally coupled with chemical looping combustion as a novel technology. Int. J. Energy Res. 39, 356–369. doi:10.1002/er.3248